Dynamic Characterization of an Alkali-Ion Battery as a Source for Laser-Cooled Atoms

J. P. McGilligan,[1,2,*] K. R. Moore,[2] S. Kang,[1,2] R. Mott,[3] A. Mis,[3] C. Roper,[3] E. A. Donley,[2] and J. Kitching[2]

[1] *Department of Physics, University of Colorado, Boulder, Colorado 80309, USA*
[2] *National Institute of Standards and Technology, Boulder, Colorado 80305, USA*
[3] *HRL Laboratories, LLC, Malibu, California 90265, USA*

(Received 13 August 2019; revised manuscript received 13 September 2019; accepted 25 March 2020; published 14 April 2020)

We investigate a solid-state reversible alkali-ion battery (AIB) capable of regulating the density of alkali atoms in a vacuum system used for the production of laser-cooled atoms. The cold-atom sample can be used with in-vacuum chronoamperometry as a diagnostic for the voltage-controlled electrochemical reaction that sources or sinks alkali atoms into the vapor. In a combined reaction-diffusion-limited regime, we show that the number of laser-cooled atoms in a magneto-optical trap can be increased both by initially loading the AIB from the vapor for longer and by using higher voltages across the AIB when atoms are subsequently sourced back into the vapor. The time constants associated with the change in atom number in response to a change in AIB voltage are in the range of 0.5–40 s. The AIB alkali reservoir is demonstrated to survive oxidization during atmospheric exposure, simplifying reservoir loading prior to vacuum implementation as a replacement for traditional resistively heated dispensers. The AIB capabilities may provide an improved atom-number stability in next-generation atomic clocks and sensors, while also facilitating fast loading and increased interrogation times.

DOI: 10.1103/PhysRevApplied.13.044038

I. INTRODUCTION

Since the demonstration of laser cooling, ensembles of laser-cooled neutral atoms have been implemented in a wide variety of precision instruments due to the long interrogation times that can be achieved without interaction with the environment. These properties are notably utilized in state-of-the-art metrological experiments, such as atom interferometers and atomic clocks [1–5]. The improved performance of these cold atom measurements compared to their thermal counterparts has led to significant efforts to miniaturize the laser-cooling apparatus into a field-deployable device [6–8].

Among the many challenges associated with moving cold-atom instrumentation from the laboratory to the field is the stabilization of the alkali-atom density. As the temperature of the environment changes, so too does the density of the alkali vapor from which the cold-atom sample is loaded. The absence of an alkali density regulator will ultimately degrade the long-term magneto-optical trap (MOT) number stability and can prevent a MOT from forming altogether for large enough deviations from room temperature. Techniques such as light-induced-atomic-desorption (LIAD) have demonstrated the ability to modulate and control the background alkali density [9,10]; however, such methods have not yet demonstrated fast desorption times, nor have they been miniaturized to facilitate portability and microfabrication [11].

Previously, we have demonstrated a low-power voltage controlled reversible device for sourcing and sinking the alkali vapor, with a graphitic carbon top electrode [11]. This microfabricated in-vacuum electrolytic device has later been utilized for stabilization of the alkali density in a vapor cell [12]. Recently, an improved generation of the AIB, which uses a fine-Pt-grid top electrode, has demonstrated that alkali atoms sourced from such a device can be laser cooled and trapped in a MOT [13].

In this paper, we evaluate in more detail how the MOT is loaded from the AIB, while simultaneously using the MOT as an *in situ* diagnostic tool to determine the characteristics of the electrochemical processes through chronoamperometry (an electrochemical technique that monitors the current response from an electrode while the applied voltage is stepped). Characterization of the AIB with a MOT is selected due to its close proximity to the device surface, while providing a measurement of the total time constants applicable for cold-atom experiments. We show that the Rb emitted into the vapor and subsequently captured by the MOT depends on both the initial state of charge within the AIB and the applied voltage during sourcing. In doing

*jpmcgilligan91@gmail.com

so, we establish how the cold-atom number and loading time depend on the operating parameters of the AIB and elucidate some of the underlying electrochemistry that determines the performance of the battery as a source for laser-cooled atomic ensembles.

II. EXPERIMENTAL SETUP

The experimental setup, as has been described in Ref. [13], is illustrated in Fig. 1(a). We create a standard six-beam MOT close to the AIB [Fig. 1(b)] with light from a single distributed-Bragg-reflector (DBR) laser, locked to address the ^{85}Rb $F = 3 \rightarrow F' = 4$ transition, while being frequency modulated at 2.9 GHz to generate approximately 10% sidebands for repumping. The light is spatially filtered using an optical fiber and provides a total incident power of 35 mW, red detuned by 2Γ, where Γ is the natural line width of the transition, and a $1/e^2$ diameter of 5 mm. The vacuum system inside the 10 mm $\times$ 10 mm $\times$ 70 mm cell is maintained with a 2 L/s ion pump and Rb can be introduced with standard heated-alkali dispensers (Rb_2MoO_4/AlZr). The cell walls are coated in octadecyltrichlorosilane (OTS) to minimize alkali adsorption [14].

The AIB, placed inside the vacuum cell, has previously been described in Ref. [13]. The internal body of the AIB houses a layer of ion-conducting Rb-β'' alumina, sandwiched between upper and lower electrodes. The upper electrode couples the Rb-β'' alumina to the outer environment via an array of electrode fingers that cover the upper surface. The lower electrode is housed within a graphite alkali reservoir, which stores neutral alkali atoms. The alkali-vapor density is enhanced when voltage is applied across the electrodes [15,16]. The bidirectional functionality to source or sink alkali atoms from the vapor is controlled by the voltage applied across the AIB and its temperature, set to 100 °C. With the exclusion of the upper electrodes and exposed Rb-β'' alumina between the top electrode features, the entire AIB surface is insulated and coated in a vacuum epoxy. MOT image acquisition is carried out with fluorescence imaging on a CCD camera.

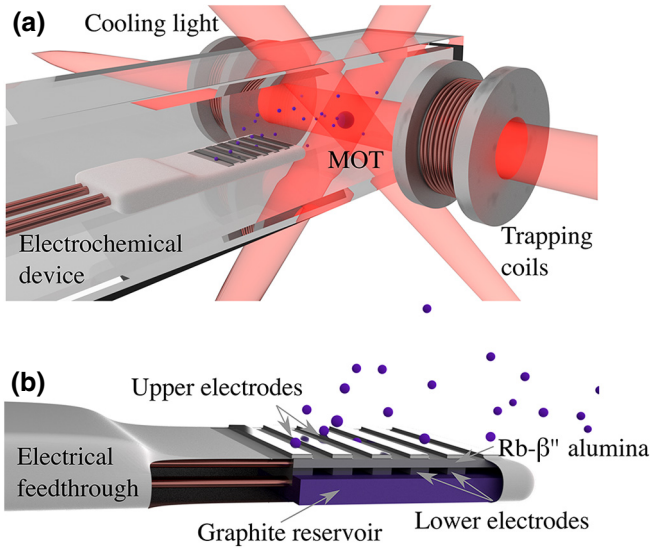

FIG. 1. (a) An illustration of the magneto-optical trap being sourced from the AIB. (b) A cut-through of the AIB is provided to reveal the internal composition.

III. RESULTS

The typical response of the measured MOT atom number N and the AIB current I to a change in the applied voltage polarity V has been described in Ref. [13] and is illustrated in Fig. 2 for clarity. The AIB is loaded with alkali atoms through the application of a negative voltage for approximately 20 s before $t = 0$ s in the presence of an alkali vapor in the cell provided by a standard heated-alkali dispenser in the hours before the experiment. The MOT light is turned on and a small number of laser-cooled atoms appears. As a positive voltage step is applied at $t = 14$ s, the number of cold atoms in the MOT is observed to increase and reaches steady state with a time constant τ_S between 0.5 s and 40 s. We note that this is not the typical MOT loading curve observed in many cold-atom experiments as a result of switching on a magnetic field gradient, described in Ref. [17], but instead reflects changes in the alkali density induced by the AIB. This increase in the number of cold atoms is associated with a sharp increase in the device current. When the polarity of the applied voltage is reversed at $t = 58$ s, the cold-atom number decays to near the detection background with time constant τ_L between 0.5 s and 10 s, again consistent with Ref. [13]. If, instead, the voltage is set to zero at $t = 58$ s, a much slower decay of the atom number is observed, with decay time constant $\tau_D \approx 100$ s. Since the MOT lifetime is significantly shorter than the measured time constants, the MOT loading process does not contribute to the measured dynamics.

The behavior shown in Fig. 2 can be explained as follows. When the positive voltage is applied, the neutral Rb at the interface of the lower electrode and graphite is ionized and conducted into the Rb-β''-alumina electrolyte as a result of the electric field created by the applied voltage. Rb^+ ions recombine with electrons at the interface between the upper electrodes and Rb-β'' alumina, producing a large initial current, while neutral Rb metal accumulates on the surface. As the electrochemical process depletes the Rb within the graphite, a Rb concentration gradient forms within the graphite, reducing the Rb density near the lower electrodes and limiting the rate of the electrochemical process by the diffusion rate of the remaining neutral Rb out of the graphitic reservoir [18,19]. The model provided in this paper well agrees with almost all aspects of Ref. [13]. However, more detailed analysis of

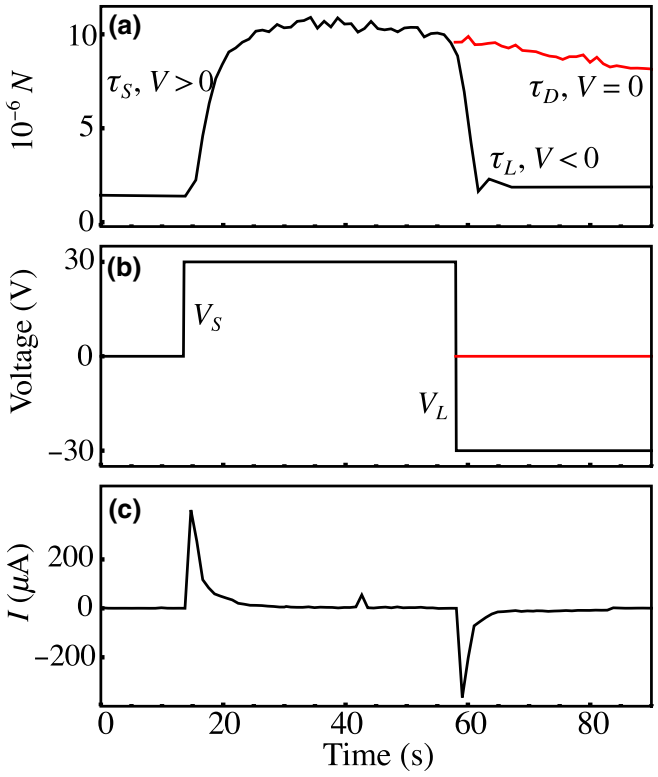

FIG. 2. (a) The number of laser-cooled atoms in the MOT, (b) the applied voltage, and (c) the corresponding current through the solid-state battery, as a function of time. At $t = 14$ s, a positive voltage is applied to the battery, causing current to flow and leading to an increase in the number of cold atoms with a time constant τ_S. At $t = 58$ s, the polarity of the applied voltage is reversed, leading to a reverse current and a decrease in the number of cold atoms with time constant τ_L. If, instead, the voltage is set to zero (red lines), the atom number decreases with the time constant τ_D. Figure adapted from Ref. [13].

the current time-series data, illustrated in Fig. 2(c), reveals a $1/\sqrt{t}$ dependence. The depleted-device electronic time constant is much faster than the observed dynamics, such that in these measurements, only the flow of Faradaic current generated at the electrode is analyzed [19,20].

By integrating the current, the total charge Q that has flowed between the upper and lower electrodes can be found. This charge represents the number of ions conducted through the Rb-β'' alumina, as permitted by electrochemical reactions at the lower and upper electrodes. Following the electrochemical process, the neutral Rb metal likely diffuses across the upper AIB surface to form a metallic film and is evaporated into the vacuum.

It is interesting to note that the response of the MOT atom number at $t = 14$ s is somewhat slower than the corresponding decay of the AIB current. We attribute this difference to the fact that in order for the alkali-vapor density (and hence the MOT atom number) to increase, the alkali metal likely diffuses on the AIB surface to form a film and subsequently evaporates into the vacuum chamber. The current flow through the AIB does not depend on these processes and if they take longer than the electrochemical processes, changes in the atomic vapor (and hence the MOT atom number) would be expected to occur more slowly.

At $t = 58$ s, the polarity of the voltage is reversed and the device switches from being a source of alkali atoms to the vapor to being a sink from the vapor. Under these conditions, vapor-phase Rb atoms that strike the upper electrodes are ionized and flow through the Rb-β'' alumina to the reservoir due to the applied electric field. The Rb^+ ions undergo reduction at the lower electrode-graphite interface and diffuse into the reservoir as neutral Rb until a source voltage is applied. If instead of sinking to the reservoir, the source voltage is simply turned off, the atom number decays at a much slower rate τ_D. We speculate that this slower decay results from a slow decrease of the metallic Rb coverage on the AIB surface due to removal of Rb from the vapor (and hence the AIB surface) by the ion pump. This reduces the rate at which alkali atoms vaporize from the surface and, combined with a constant pumping rate from the ion pump, results in a lower overall Rb density in the vapor.

A. AIB loading time

The number of atoms in the MOT depends on the time duration over which atoms are initially loaded into the AIB, t_L. To ensure a repeatable initial state of the experiment, a positive voltage is applied across the AIB to deplete any previously stored Rb from the reservoir. Prior to the set of AIB loading-time measurements, the alkali dispenser is heated to temporarily increase the Rb pressure in the vacuum chamber. For each loading time tested, Rb is loaded into the AIB by applying −30 V to the AIB electrodes for a variable time duration. Following loading, the voltage is briefly turned off; then the polarity is reversed and atoms are sourced from the AIB at 30 V while monitoring the fluorescence from the MOT. The applied voltage as a function of time and the corresponding number of atoms detected in the MOT are shown in Figs. 3(a) and 3(b). Figure 3(c) shows that the peak atom number, N_{Peak}, measured for a constant source voltage, increases with t_L between 10 s and 1000 s. We note that for the larger loading-time durations, there is indication that the reservoir concentration has saturated. The total time over which the atom number remains at steady state t_{SS}, defined by the time taken for the peak atom number to decrease by 25%, is seen to be consistent with a $\sqrt{t_L}$ dependence, as shown in Fig. 3(d), where the black line is a square-root function. The total charge between the electrodes, determined by integrating the area under the current during the first 50 s of sourcing, is observed to increase as $\sqrt{t_L}$ over this same increase in loading-time duration, as illustrated

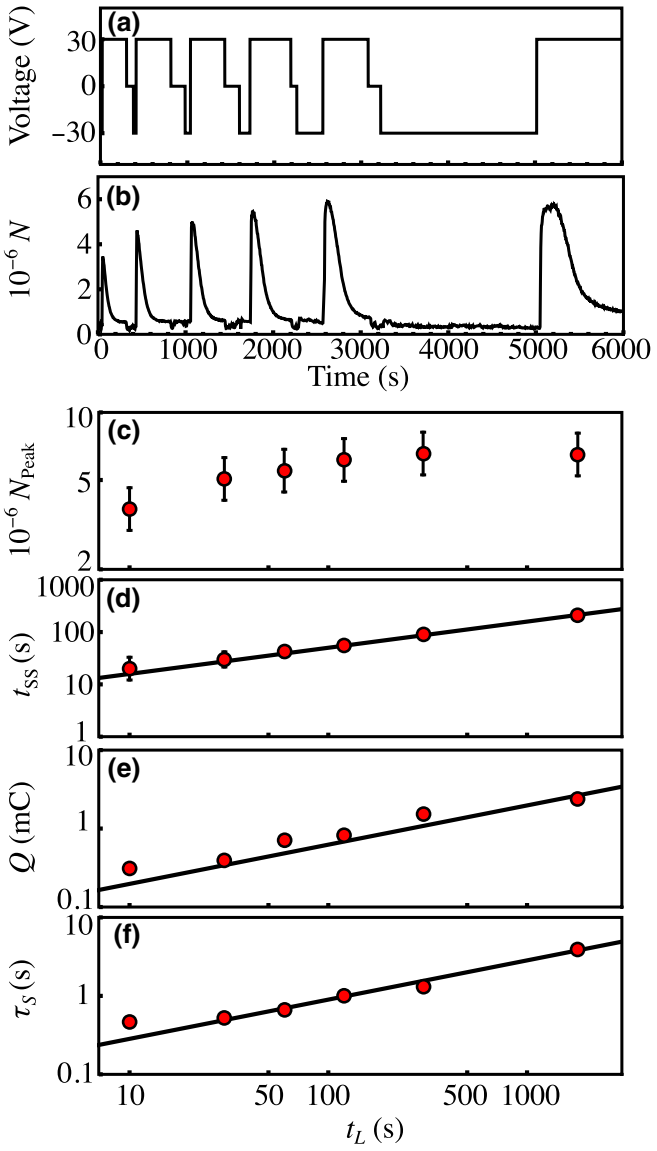

FIG. 3. The device performance as a function of the time during which the device loads atoms from the vapor. (a) The voltage applied across the device as a function of time, showing five experimental cycles of loading at −30 V followed by sourcing at +30 V. The time during which the device loads atoms at −30 V is increased with each subsequent cycle. (b) The number of cold atoms in the MOT increases for longer loading times. (c) The peak atom number, (d) the time over which the MOT number remains at steady state, (e) charge transferred across the AIB (measured by integrating the current pulse), and (f) the time constant for the MOT atom number to reach steady state after application of the sourcing voltage, τ_S. Black lines represent the fit of a $\sqrt{t_L}$ dependence.

in Fig. 3(e). Figure 3(f) illustrates that the time for the MOT number to reach steady state, τ_S, is also consistent with a $\sqrt{t_L}$ function of the loading-time duration.

Longer durations of loading time at the same loading voltage should result in a larger number of neutral Rb atoms entering the device and hence a higher density of Rb within the reservoir. Such an increased Rb content produces a larger total charge during sourcing under the same sourcing voltage, leading to the formation of a larger number of Rb-metal atoms on the surface and greater device surface coverage. This results in an increased evaporation rate and a larger Rb vapor density and MOT number. The reason why τ_S increases with the AIB loading time requires further investigation but is possibly due to the atoms penetrating deeper within the reservoir. The measured increase of the sourced atom number and charge transfer indicates that the peak atom number for a constant applied voltage is dictated by the bulk concentration within the reservoir.

We find that Rb can be stored within the AIB reservoir during exposure to the atmosphere. Rb is loaded into the AIB from a background alkali density before exposure to the atmosphere for 1 h. Following this exposure, the vacuum is reestablished below 10^{-8} mbar in the chamber and when a sourcing voltage is applied to the AIB, the MOT can be loaded, demonstrating the ability to store pure metallic Rb in oxygen and water vapor containing an atmosphere without complete Rb oxidation.

B. AIB sourcing voltage

The MOT atom number and loading time depend on the applied sourcing voltage for constant loading conditions. The voltage across the AIB is set to −30 V to load Rb from the vacuum for 30 min. Subsequently, a positive voltage V_S is applied, as illustrated in Fig. 4(a), resulting in the formation of a MOT with a steady-state number N_{SS} and a time constant τ_S, as shown in Fig. 4(b). The voltage is then set to 0 V and the background alkali density is allowed to fall back to its initial level. This procedure is repeated for five voltages. For an electrochemical reaction contribution, the current is expected to have an exponential dependence on the applied voltage by means of the Butler-Volmer equation [21]. An exponential relation between the applied voltage and measured steady-state current is observed from this data set, illustrated in Fig. 4(c). If the AIB were purely diffusion limited and not reaction limited, then the current would be independent of the applied voltage. Instead, an exponential relation is found, which indicates that when in the regime of an increasing voltage, the AIB is not entirely diffusion-limited and is instead in a regime where there is a significant contribution from the electrochemical reaction process.

The steady-state atom numbers that are measured following sourcing are plotted in Fig. 4(d) as a function of the AIB applied voltage, where the black line represents the best power-law fit. The results demonstrate a larger number of sourced Rb for higher applied voltages and higher currents. In the case of sourcing, we find that the data are consistent with $N_{SS} \propto V_S$. Again, the MOT number is demonstrated to be correlated with the Rb^+ charge into and

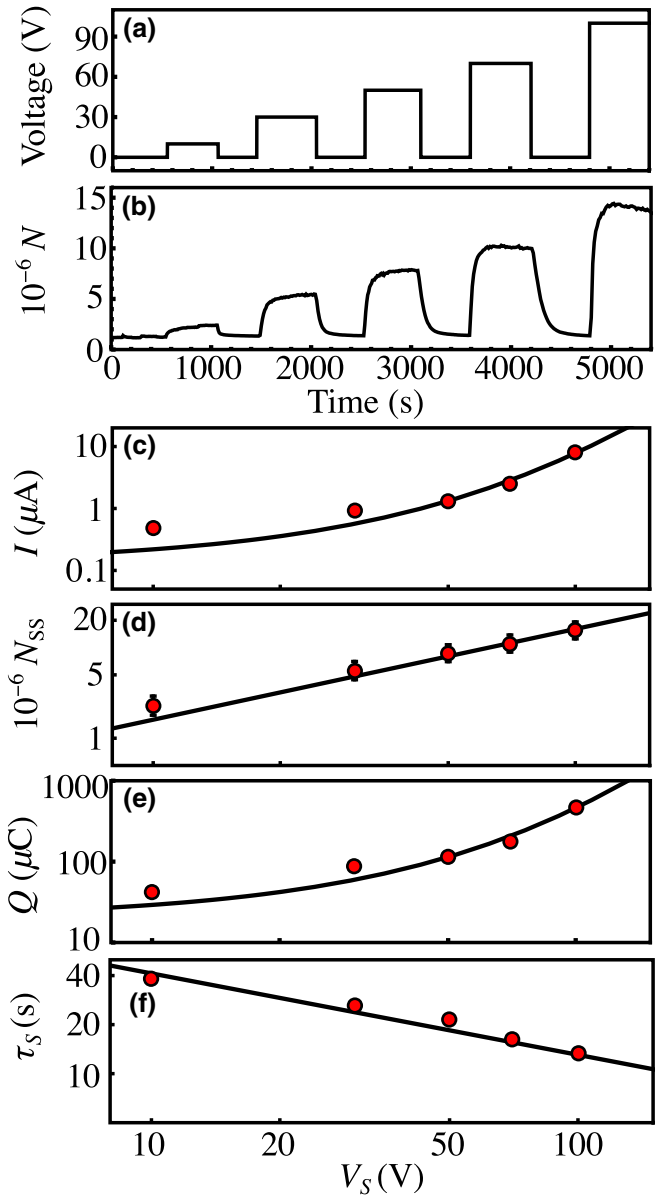

FIG. 4. The device performance as a function of the steady-state source voltage. (a) The raw time-domain data of the applied voltage. (b) The raw time-domain data of the atom-number sourcing. (c) The steady-state current. (d) The steady-state MOT number. (e) The charge during the first 50 s of sourcing. (f) The sourcing time constant, τ_S. Black lines indicate the best fit to the data with the functional forms described in the text.

out of the Rb-β'' alumina, illustrated in Fig. 4(e), where we see an exponential increase in the charge over the range of voltages from 10 V to 100 V.

The time constant τ_S, shown in Fig. 4(f), decreases with $1/\sqrt{V_S}$, as highlighted by the black-line square-root fit. The faster time constant would be expected for a faster electrochemical recombination process generated by the higher potential at larger voltages. However, the long time constants observed here may be the result of a secondary process that increases τ_S. The cause of this is not entirely known, but it could possibly be caused by Rb diffusion on the top surface of the device prior to evaporation. In this scenario, the increased charge is due to the larger applied voltage during sourcing providing an increased potential to aid a faster electrochemical recombination rate at the surface. However, we note that although the total source time is less than the total load time, there may be an effect of reservoir depletion visible toward the end of the experiment, highlighted by the decreasing atom number from steady state at $t = 5000$ s in Fig. 4(b).

C. AIB loading voltage

If the voltage across the AIB is reversed while trapped atoms are present, the atom number in the MOT decays with the time constant τ_L, as shown in Fig. 5(a). We measure this time constant as a function of the applied loading voltage by first sourcing the AIB at 30 V until the atom number reaches steady state. The polarity of the applied voltage is reversed, permitting measurement of τ_L and the current drawn by the device as the AIB pumps away the alkali vapor in the chamber. This procedure is carried out for a number of loading voltages, each time ensuring that the starting background density and pressure are constant, as well as the sourcing voltage and steady-state MOT number. Three examples of raw results of this data set are plotted in Fig. 5(a), with the full data sets of τ_L as a function of the voltage shown in Figs. 5(b), 5(c), 5(d), and 5(e). As would be expected from the reaction rate contribution during sourcing, the steady-state loading current is also exponential with the applied voltage [Fig. 5(b)], indicating that both loading and sourcing have a contribution from an electrochemical reaction rate. While the change in atom number ΔN is nominally independent of the loading voltage due to the similar initial conditions of each experiment, small variations occur from shot to shot due to slowly varying experimental parameters as a result of environmental fluctuations in the laboratory. We find that the AIB charge transferred during the first 10 s of loading produces a 47% fluctuation from the mean, relating to a 34% fluctuation with the measured change in cold-atom number, as shown in Figs. 5(c) and 5(d). A correlation coefficient of 0.82, along with the relative insensitivity of the charge transfer to the applied loading voltage, indicates that the number ofRb^+ ions that sink in and out of the Rb-β'' alumina in a given time are proportional to the MOT and background Rb density level present during loading. As the loading voltage is increased, a faster electrochemical reaction process is demonstrated for the AIB, consistent with a $\tau_L \propto V_L^{-1.5}$, as shown in Fig. 5(e), where the black line is a best power-law fit. For the largest loading voltages, τ_L appears to saturate with a minimum of $\tau_L = 540$ ms, while the applied voltage continues to increase. For this reason, these data points are not included in the fit. This

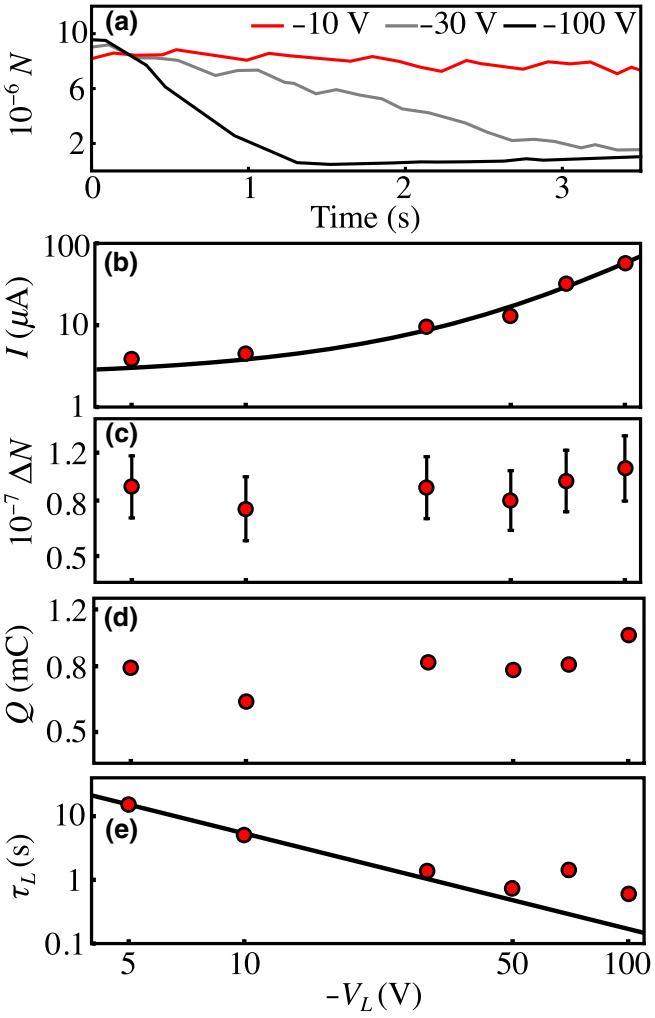

FIG. 5. The measured parameters for the steady-state AIB loading current. (a) The raw time-domain data of the atom number during loading with −10 V, −30 V, and −100 V in red, gray, and black, respectively. (b) The steady-state current. (c) The change in MOT number during loading. (d) The charge transfer during the first 10 s of loading. (e) The loading time constant, τ_L. Black lines indicate the best fit to the data with the functional forms described in the text.

saturation indicates that the process is limited by a time constant prior to the electrochemical disassociation, such as the diffusion of metal Rb upon the AIB upper surface. At the highest loading voltages of −100 V, we are able to sink Rb over 200 times faster than $\tau_D = 130$ s in Fig. 2(a), taken with zero applied loading voltage. The short time constant for decreasing the background alkali density can enable rapid loading of a MOT at high background alkali density, followed by long trap lifetimes after subsequent rapid removal of the vapor by the AIB.

IV. CONCLUSION

Alkali ion batteries can be used to store, source, and sink alkali atoms in instruments based on laser-cooled atomic ensembles. We demonstrate here that the density of an alkali vapor and hence the number of atoms in a magneto-optical trap can be controlled by the conditions over which the battery is operated. Increasing the time over which alkali atoms are initially loaded into the AIB results in larger MOT numbers upon subsequent sourcing to the vapor but also implies longer sourcing time constants. Increasing the sourcing voltage also leads to a larger number of trapped atoms but with shorter sourcing time constants. By combining these parameters, it is likely that a long loading time and a subsequent large source voltage can provide the best of both worlds, with a large atom number and simultaneously a fast time constant. Finally, depletion of atoms from the vapor and MOT depends strongly on the loading voltage and can be made as low as 540 ms under optimal conditions with the current device design. The reversible functionality demonstrated by the device makes it a good candidate for stabilizing the MOT number in a fluctuating background density or temperature environment. In addition, the AIB is able to preserve the alkali atoms stored in it upon exposure to air and is able to successfully source atoms upon subsequent introduction into a suitable vacuum.

The results also allow us to elucidate some aspects of the device operation. It appears that both electrochemical reaction and diffusion within the device or on the surface contribute to the transfer of atoms between the vapor and the reservoir. Changes in electrode design may therefore improve the overall device time constants by enabling faster Rb transport on the device surface. It is not yet clear what the capacity of the device to store Rb is, since only slight indications of saturation in the MOT atom number are evident for the range of device parameters that we explore. The ultimate capacity of the device to store Rb will also be explored in future research.

ACKNOWLEDGMENTS

This material is based upon work supported by the Defense Advanced Research Projects Agency (DARPA) and the Space and Naval Warfare Systems Center Pacific (SSC Pacific) (Contract No. N66001-15-C-4027). J.P.M. gratefully acknowledges support from the English Speaking Union and Lindemann Fellowship. The authors acknowledge Logan Sorenson, Matthew Rakher, Jason Graetz, John Vajo, Adam Gross, and Danny Kim of HRL Laboratories, LLC for useful discussions. They further acknowledge Florian Herrault, Geovanni Candia, Stephen Lam, Tracy Boden, Margie Cline, Ryan Freeman, and Lian-Xin Coco Huang for assistance with device fabrication. They thank Vincent Maurice and Yun-Jhih Chen for their comments on the manuscript.

J. P. McGilligan, K. R. Moore, and S. Kang conceived and carried out the experiments, supervised by J. Kitching and E. A. Donley. J.P.M. wrote the manuscript, with

critical input from K.R.M., J.K., E.A.D., and C.R. C.R. conceived and designed the alkali-ion battery. R.M., A.M., and C.R. fabricated the alkali-ion battery. All authors reviewed the manuscript.

The authors declare that they have no competing interests. Approved for Public Release, Distribution Unlimited.

[1] A. D. Ludlow and J. Ye, Progress on the optical lattice clock, Competes Rendus Physique **16**, 499 (2015).

[2] M. Takamoto, F. L. Hong, R. Higashi, and H. Katori, An optical lattice clock, Nature **435**, 321 (2005).

[3] A. Arvanitaki, S. Dimopoulos, A. A. Geraci, J. Hogan, and M. Kasevich, Testing Atom and Neutron Neutrality with Atom Interferometry, Phys. Rev. Lett. **100**, 120407 (2008).

[4] A. G. Rosi, F. Sorrentino, L. Cacciapuoti, M. Prevedelli, and G. M. Tino, Precision measurement of the Newtonian gravitational constant using cold atoms, Nature **510**, 518 (2014).

[5] Y. Zhai, C. H. Carson, V. A. Henderson, P. F. Griffin, E. Riis, and A. S. Arnold, Talbot-enhanced, maximum-visibility imaging of condensate interference, Optica **5**, 80 (2018).

[6] J. A. Rushton, M. Aldous, and M. D. Himsworth, Contributed review: The feasability of a fully miniaturized magneto-optical trap for portable ultracold quantum technology, Rev. Sci. Rep. **85**, 121501 (2014).

[7] A. T. Dellis, M. T. Hummon, S. Kang, E. A. Donley, and J. E. Kitching, Chip-scale MOT for microsystems technology, Front. Opt. (2016).

[8] J. P. McGilligan, P. F. Griffin, R. Elvin, S. J. Ingleby, E. Riis, and A. S. Arnold, Grating chips for quantum technologies, Sci. Rep. **7**, 384 (2017).

[9] L. Torralbo-Campo, G. D. Bruce, G. Smirne, and D. Cassettari, Light-induced atomic desorption in a compact system for ultracold atoms, Sci. Rep. **5**, 14729 (2015).

[10] T. Karaulanov, M. T. Graf, D. English, S. M. Rochester, Y. J. Rosen, K. Tsigutkin, D. Budker, E. B. Alexandrov, M. V. Balabas, D. F. J. Kimball, F. A. Narducci, S. Pustelny, and V. V. Yashchuk, Controlling atomic vapor density in paraffin-coated cells using light-induced atomic desorption, Phys. Rev. A **79**, 012902 (2009).

[11] S. Kang, R. P. Mott, K. A. Gilmore, L. D. Sorenson, M. T. Rakher, E. A. Donley, J. E. Kitching, and C. S. Roper, A low-power, reversible alkali atom source, Appl. Phys. Lett. **110**, 244101 (2017).

[12] S. Kang, R. P. Mott, A. Mis, C. S. Roper, E. A. Donley, and J. E. Kitching, Active stabilization of alkali-atom vapor density with a solid-state electrochemical alkali-atom source, Opt. Express **26**, 3696 (2018).

[13] S. Kang, K. R. Moore, J. P. McGilligan, R. P. Mott, A. Mis, C. S. Roper, E. A. Donley, and J. E. Kitching, A magneto-optic trap using a reversible, solid-state alkali-metal source, Opt. Lett. **44**, 3002 (2019).

[14] S. J. Seltzer and M. V. Romalis, High-temperature alkali vapor cells with antirelaxation surface coatings, J. Appl. Phys. **106**, 114905 (2009).

[15] F. Gong, Y. Y. Jau, K. Jensen, and W. Happer, Electrolytic fabrication of atomic clock cells, Rev. Sci. Instrum. **77**, 076101 (2006).

[16] J. J. Bernstein, S. Feller, A. Ramm, J. North, J. Maldonis, M. Mescher, W. Robbins, R. Stoner, and B. Timmons, All solid state ion-conducting cesium source for atomic clocks, Solid State Ionics **198**, 47 (2011).

[17] K. Lindquist, M. Stephens, and C. Wieman, Experimental and theoretical study of the vapor-cell Zeeman optical trap, Phys. Rev. A **46**, 7 (1992).

[18] D. A. C. Brownson and C. E. Banks, *The Handbook of Graphene Electrochemistry* (Springer, London, 2015).

[19] A. Molina and J. Gonzalez, *Pulse Voltammetry in Physical Electrochemistry and Electroanalysis: Theory and Applications* (Springer International, 2015).

[20] F. C. Anson, Innovations in the study of adsorbed reactants by chronocoulometry, Anal. Chem. **38**, 54 (1966).

[21] A. J. Bard and L. R. Faulkner, *Electrochemical Methods: Fundamentals and Applications* (Wiley, 2001), 2nd ed.